AIP | Journal of Applied Physics

Unique properties of CuZrAl bulk metallic glasses induced by microalloying

B. Huang, H. Y. Bai, and W. H. Wang

Citation: J. Appl. Phys. **110**, 123522 (2011); doi: 10.1063/1.3672449
View online: http://dx.doi.org/10.1063/1.3672449
View Table of Contents: http://jap.aip.org/resource/1/JAPIAU/v110/i12
Published by the American Institute of Physics.

JOURNAL OF APPLIED PHYSICS **110**, 123522 (2011)

Unique properties of CuZrAl bulk metallic glasses induced by microalloying

B. Huang, H. Y. Bai, and W. H. Wang[a)]
Institute of Physics, Chinese Academy of Sciences, Beijing 100080, People's Republic of China

(Received 14 September 2011; accepted 21 November 2011; published online 27 December 2011)

We studied the glass forming abilities (GFA), mechanical, and physical properties of $(CuZr)_{92.5}Al_7X_{0.5}$ (X = La, Sm, Ce, Gd, Ho, Y, and Co) bulk metallic glasses (BMGs). We find that the GFA, mechanical, and physical properties can be markedly changed and modulated by the minor rare earth addition. The Kondo screening effect is found to exist in $(CuZr)_{92.5}Al_7Ce_{0.5}$ BMG at low temperatures and the Schottky effect exists in all the rare earth element doped BMGs. Our results indicate that the minor addition is an effective way for modulating and getting desirable properties of the BMGs. The mechanisms of the effects of the addition are discussed. The results have implications for the exploration of metallic glasses and for improving the mechanical and low temperature physical properties of BMGs.
[doi:10.1063/1.3672449]

I. INTRODUCTION

Compared to traditional crystalline metallic materials, bulk metallic glasses (BMGs) with atomically amorphous structure exhibit unique physical, chemical, and mechanical properties and have attracted world-wide interest for the opening of new opportunities for fundamental research and commercial applications.[1–3] Great progress in basic research and applications have been achieved while many issues remain unsolved.[1–3] Minor addition or microalloying technique, which has been widely used in metallurgical fields, plays important roles in formation and property improvement of BMGs.[4] For example, the centimeter-sized BMGs based on ordinary transition metals Fe, Cu, Zr, noble metal Pd, light metal Mg and rare earth metal Ce have been developed through this method.[4–6] Composites with better mechanical or physical properties, Fe-based glass-forming alloys with improved soft magnetic properties and Zr-based, TiCu-based BMGs with enhanced plasticity have been obtained by minor addition of fibers, nanotubes, particles, metalloid, and metallic elements.[4–6]

Since the first report of the successful preparation of Cu_xZr_{100-x}($45 < x < 60$ at.%) BMGs with a 2 mm diameter,[7–10] the CuZr and CuZr-based BMGs have become model systems for studying the glass forming abilities (GFA), structural characteristics, and mechanical and physical properties in metallic glasses. A great deal of work has been done on their formation, deformation and mechanical properties.[11–15] The improvement of the CuZr-based BMGs through minor addition was proposed to be associated with the factors of oxygen scavenging effect,[16] decrease of long range atomic diffusion,[17] suppression of dendrite phase precipitation,[18] better symmetry of clusters,[19] and low density of electronic energy states at the Fermi level.[20] Minor Ti or Fe addition can enhance the plasticity of CuZrAl BMGs due to the creation of a large amount of free volume and phase separation.[21,22] Yu and Bai. found that $(CuZr)_{100-x}Al_x$ ($0 < x < 10$) BMGs with largest plasticity also have the maximum Poisson's ratio.[23] However, little work has been done on the effects of minor addition on the physical properties especially low temperature properties such as the tunneling states, boson peak, magnetic properties in CuZr and CuZr-based BMGs.[24–26]

Rare earth (RE) and transition metal elements are important minor addition materials that have unique and important impacts on the formation, structure, and properties of BMGs.[4] Since the RE elements and some transitional elements such as Co have plentiful and unique physical properties, and the BMGs with addition of these elements could be of potential for application as functional materials.[3,27,28] The La, Ce, Sm, Gd, Ho, and Y elements have very close enthalpies with Cu, Zr, and Al elements[29] and nearly the same outside electronic layers.[27] The Ce, Sm, Gd, and Ho atoms have gradually increasing 4*f* electrons and different magnetic properties. The cobalt has magnetism mainly due to its 3*d* itinerant electrons, which is different from rare earth elements.[28] The effects of minor addition of these elements into CuZr-based BMGs on low temperature physical properties could be unique and interesting.

In this work, we systematically investigated the effects of the addition of less than 1 at.% La, Ce, Sm, Gd, Ho, Y, and Co on the GFA and mechanical and physical properties of the CuZr-based BMGs. We find that the addition induces unique and important impact on the formation, structure and low temperature physical properties of the BMGs. The physical mechanisms for the found phenomena are carefully discussed.

II. EXPERIMENTAL DETAILS

Ingots with nominal compositions of $(CuZr)_{92.5}Al_7X_{0.5}$ (X = La, Ce, Sm, Gd, Ho, Y, and Co) were prepared by arc-melting the mixture of high-purity elements under Ti-gettered argon atmosphere. Each ingot was remelted for more than four times to ensure the homogeneity of the composition and then was injected into a copper mold to obtain a cylindrical rod of 2 mm in diameter. The total mass of the remaining ingot and rod was weighed to insure that the loss of the added element was less than 5%. The content of the added element

a)Author to whom correspondence should be addressed. Electronic mail: whw@iphy.ac.cn.

was then confirmed by chemical analysis. The amorphous structure of the as-cast rods was ascertained by an Ultima IV X-Ray diffractometer with Cu K_α rays at 40 kV. Thermal dynamic properties were examined using the NETZSCH DSC 404F3 Pegasus under argon atmosphere with a heating rate of 10 K min^{-1}. Room temperature compressive tests were carried out in an Instron electromechanical 3384 test system at a strain rate of 1×10^{-4} s^{-1} with cylindrical rods in a 4 mm length and a 2 mm diameter. More than three rods were tested for each BMG sample. The temperature and field dependence of specific heat capacity and resistance were measured by PPMS 6000 of Quantum Design Company. Magnetic properties were tested in MPMS (SQUID)-VSM 7 T System of Quantum Design Company.

III. RESULTS AND DISCUSSIONS

A. The effects of minor addition on formation and mechanical properties

The fully amorphous structure of $(CuZr)_{92.5}Al_7X_{0.5}$ (X = La, Ce, Sm, Gd, Ho, Y, and Co) alloys with a 2 mm diameter are identified by the X-ray diffraction (XRD) patterns (as shown in Fig. 1). These BMGs with different minor additions have slightly but distinguished different first hump. This indicates that the minor addition with different elements induces different short-range structures in the BMG. As an example, Fig. 2(a) shows the differential scanning calorimetric (DSC) curve of $(CuZr)_{92.5}Al_7Co_{0.5}$ BMG. The distinct glass transition peak in the DSC trace further confirms the full glassy structure of the additional BMG. The glass transition temperatures (T_g), crystallization temperatures (T_x), melting points (T_m), liquidus temperatures (T_l) of $(CuZr)_{92.5}Al_7X_{0.5}$ (X = La, Ce, Sm, Gd, Ho, Y, and Co) BMGs determined by DSC are shown in Figs. 2(b) and 2(c). Melting points of the added elements $T_{m\text{-}el}$, and T_g, T_x, T_m, T_l, supercooled liquid regions ΔT_x $(=T_x - T_g)$, reduced glass transition temperatures $T_{rg}(=T_g/T_l)$, and $\gamma(=T_x/(T_g+T_l))$ of the BMGs are listed in Table I.

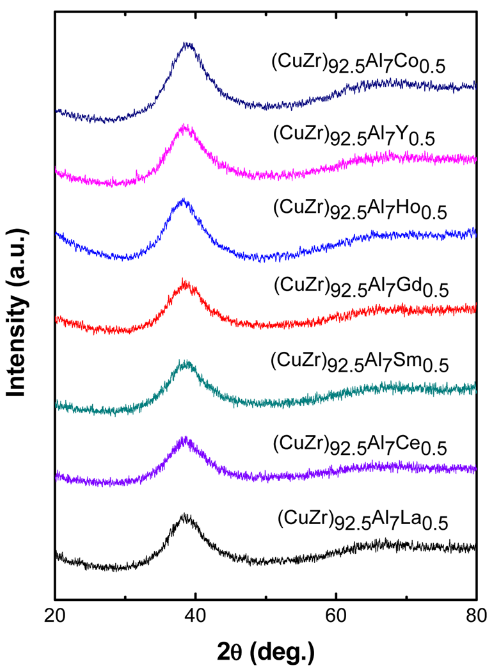

FIG. 1. (Color online) XRD diffraction patterns of $(CuZr)_{92.5}Al_7X_{0.5}$ (X = La, Ce, Sm, Gd, Ho, Y, and Co) glassy rods with a 2 mm diameter.

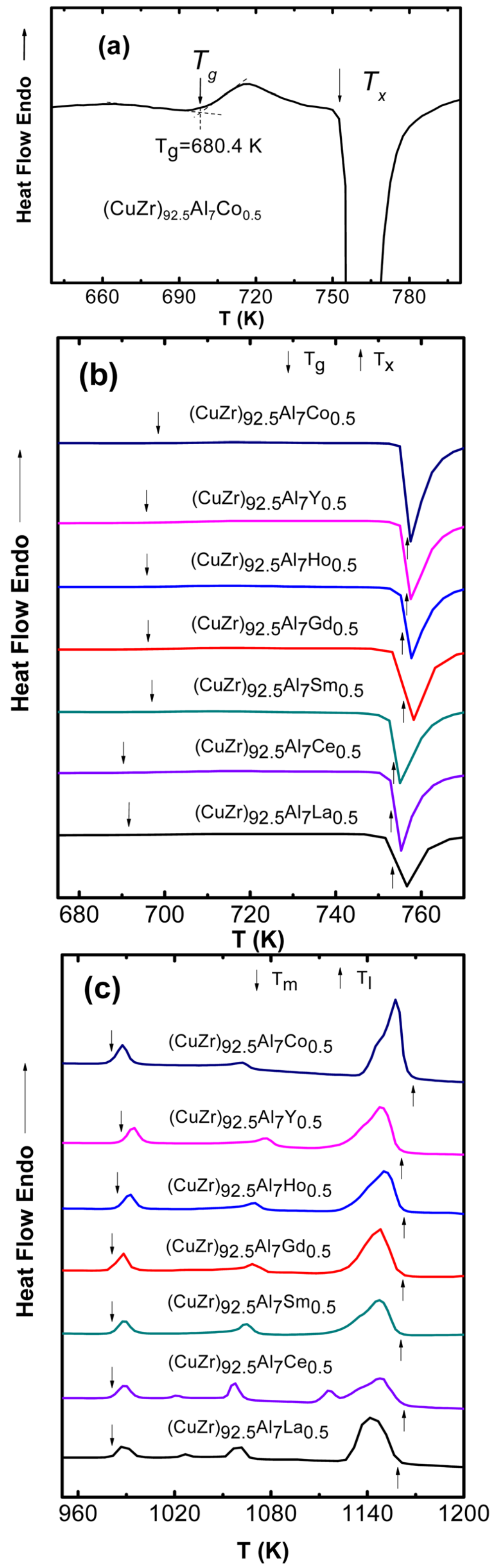

FIG. 2. (Color online) DSC curves of $(CuZr)_{92.5}Al_7X_{0.5}$ (X = La, Ce, Sm, Gd, Ho, Y, Co) BMGs with a heating rate of 10 K/min. (a) The glass transition peak of the BMG. (b) Glass transition and crystallization. (c) Melting.

TABLE I. Melting temperature of the added elements $T_{m\text{-}el}$ and thermodynamic data of $(CuZr)_{92.5}Al_7X_{0.5}$ (X = Ce, La, Sm, Gd, Ho, Y, and Co) BMGs. The data of $(CuZr)_{93}Al_7$ BMG are also presented for comparison.

Alloys	$T_{m\text{-}el}$ (K)	T_g (K)	T_x (K)	T_m (K)	T_l (K)	ΔT_x (K)	T_{rg}	γ
$(CuZr)_{93}Al_7$	–	697	762	981	1169	66	0.596	0.409
$(CuZr)_{92.5}Al_7Ce_{0.5}$	1072	690	753	981	1163	63	0.593	0.406
$(CuZr)_{92.5}Al_7La_{0.5}$	1193	692	753	981	1159	62	0.597	0.407
$(CuZr)_{92.5}Al_7Sm_{0.5}$	1345	697	754	981	1161	57	0.601	0.406
$(CuZr)_{92.5}Al_7Gd_{0.5}$	1587	696	756	981	1162	60	0.599	0.407
$(CuZr)_{92.5}Al_7Ho_{0.5}$	1745	696	756	984	1162	60	0.599	0.407
$(CuZr)_{92.5}Al_7Y_{0.5}$	1799	696	757	987	1161	61	0.599	0.407
$(CuZr)_{92.5}Al_7Co_{0.5}$	1768	698	757	980	1168	58	0.598	0.405

From Fig. 2(c) we can see that $(CuZr)_{92.5}Al_7X_{0.5}$ BMGs have different melting behavior with the different minor addition. Especially, the La and Ce addition induces an anomalous broad melting peak. Xu *et al.*[17] found that $Cu_{45}Zr_{48\text{-}x}Al_7RE_x$ (RE = La, Ce and x = 2, 3, 5 at.%) alloys had worse GFA compared to that of $Cu_{45}Zr_{48}Al_7$ alloy while minor Gd and Y addition could improve the GFA of the CuZrAl alloy.[17,18] The phenomenon was due to the different perceptibility of RE-related (RE = La, Ce, Gd) crystalline phases from undercooled liquid according to RE-Cu, RE-Zr, RE-Al phase diagrams.[16] The anomalous melting peaks of $Cu_{45}Zr_{48\text{-}x}Al_7RE_x$ (RE = La, Ce) might correlate with the melting of the different crystallized phases. As shown in Table I, $(CuZr)_{92.5}Al_7X_{0.5}$ (X = La, Sm, Gd, Ho, Y, and Co) BMGs all have lower ΔT_x, γ and higher T_{rg} than that of $(CuZr)_{93}Al_7$ BMG. Proper addition (~ 2%) of Gd and Y can significantly improve the GFA of CuZrAl BMGs for the scavenging of oxygen, hindering of copper diffusion, and suppression of the growth of eutectic clusters and precipitation of primary dendrite phase.[17,18] As shown in Fig. 2 and Table I, the T_g, T_x, and T_m of the $(CuZr)_{92.5}Al_7X_{0.5}$ (X = Ce, La, Sm, Gd, Ho, and Y) BMGs have minor changes with the addition of the elements.

Figure 3 shows the room temperature engineering stress–strain curves of $(CuZr)_{92.5}Al_7X_{0.5}$ (X = La, Ce, Sm, Gd, Ho, Y, and Co) BMGs under compression. Table II lists the atomic radii of the addition elements r_{el}, Young's modulus E, yielding stresses σ_y, ultimate breaking stresses σ_{max}, and plastic strains ε_p of these BMGs. One can see that the $(CuZr)_{92.5}Al_7X_{0.5}$ BMGs (X = Gd, Y, Co) show slight plasticity while $(CuZr)_{92.5}Al_7X_{0.5}$ (X = La, Ce, Sm) BMGs are extremely brittle.

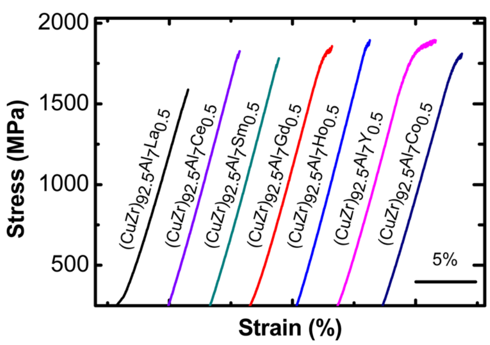

FIG. 3. (Color online) Compressive engineering stress–strain curves of $(CuZr)_{92.5}Al_7X_{0.5}$ (X = La, Ce, Sm, Gd, Ho, Y, and Co) BMGs.

TABLE II. Atomic radii of added elements r_{el} and mechanical data for $(CuZr)_{92.5}Al_7X_{0.5}$ (X = La, Ce, Sm, Gd, Ho, Y and Co) BMGs.

Alloys	r_{el} (nm)	E (GPa)	σ_y (MP)	σ_{max} (MP)	ε_p (%)
$(CuZr)_{92.5}Al_7La_{0.5}$	0.187	52.5	–	1589	–
$(CuZr)_{92.5}Al_7Ce_{0.5}$	0.182	57.3	–	1825	–
$(CuZr)_{92.5}Al_7Sm_{0.5}$	0.180	58.4	–	1781	–
$(CuZr)_{92.5}Al_7Gd_{0.5}$	0.180	56.4	1830	1857	0.08
$(CuZr)_{92.5}Al_7Ho_{0.5}$	0.176	59.8	–	1893	–
$(CuZr)_{92.5}Al_7Y_{0.5}$	0.180	56.8	1800	1894	0.72
$(CuZr)_{92.5}Al_7Co_{0.5}$	0.125	50.7	1785	1810	0.06

tle. All the BMGs have high elastic strains of about 2% while for crystalline metals elastic strains are normally no more than 0.5%.[30] For polycrystalline metals, their Young's modulus can be expressed as $2\alpha ze^2/a^3$, where α is the Madelung constant, z is the elementary charge, e is the number of valence electrons, a is the equilibrium distance between a pair of adjacent negative and positive charges.[31] So, the Young's modulus of polycrystalline metals is proportional to their valence electron densities. The La, Ce, Sm, Gd, Y, and Ho atoms with decreasing atomic radiuses all have three valence electrons,[27,32] and then the $(CuZr)_{92.5}Al_7RE_{0.5}$ (RE = La, Ce, Sm, Gd, Ho, and Y) BMGs have increasing valence electron densities supposing atoms stack compactly in BMGs. Interestingly, it is found that the Young's modulus and ultimate stresses of these BMGs indeed increase with the decrease of the atomic radius of the additional element that is correlated with their valence electron densities (see Fig. 4).

B. The effects of minor addition on low temperature properties

1. Boson heat capacity

The inset of Fig. 5 shows the specific heat versus temperature between 2 and 40 K under magnetic field of 0 T for

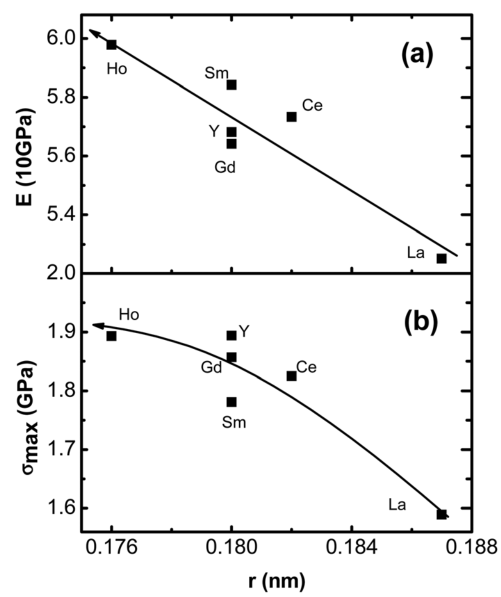

FIG. 4. Young's modulus E and ultimate fracture stress σ_{max} vs the added element's radius r_{el} for $(CuZr)_{92.5}Al_7X_{0.5}$ (X = La, Ce, Sm, Gd, Ho, and Y) BMGs. The curves with arrows are drawn as a guide for the eyes.

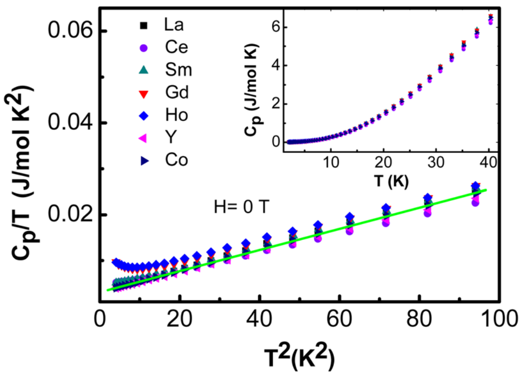

FIG. 5. (Color online) C_p/T vs T^2 between 2 and 10 K with the inset showing C_p vs T between 2 and 40 K at 0 T for $(CuZr)_{92.5}Al_7X_{0.5}$ (X = La, Ce, Sm, Gd, Ho, Y, and Co) BMGs.

$(CuZr)_{92.5}Al_7X_{0.5}$ (X = La, Co, Ce, Gd, Ho, Sm, and Y) BMGs. No obvious peaks are observed indicating that no magnetic phase transitions occur. The specific heat of $(CuZr)_{92.5}Al_7X_{0.5}$ (X = La, Y, and Co) BMGs between 2 and 10 K can be fitted well by the formula $C_p = \gamma_e T + \beta T^3$, where γ_e represents the Sommerfeld coefficient. However, for C_p/T versus T^2 plots of $(CuZr)_{92.5}Al_7X_{0.5}$ (X = Ce, Sm, Gd, and Ho) BMGs upturns appear below 4 K (as shown in Fig. 5), which could be due to magnetic cluster vibrations, Schottky effect, and Kondo effect.[33–35]

Figure 6 shows the boson heat capacity peaks of $(CuZr)_{92.5}Al_7X_{0.5}$ (X = La, Ce, Sm, Gd, Ho, Y, and Co) BMGs. For $(CuZr)_{92.5}Al_7X_{0.5}$ (X = La, Y, and Co) BMGs, we got the Sommerfeld coefficient γ_e from the least-square linear fit of specific heat data with the formula $C_p = \gamma_e T + \beta T^3$ below 10 K. As to $(CuZr)_{92.5}Al_7X_{0.5}$ (X = Ce, Sm, Gd, Ho) BMGs, we obtained γ_e in low temperature range where the Kondo and/or Schottky effect is small with formula $C_p = \gamma_e T + \beta T^3 + C$, in which C represents the constant contribution of magnetic clusters. The boson specific heat of $(CuZr)_{92.5}Al_7X_{0.5}$ (X = La, Ce, Sm, Gd, Ho, Y, and Co) BMGs is obtained after subtracting electronic and/or magnetic cluster contributions from the total specific heat. The γ_e, β, boson heat capacity temperatures T_{max} and peak intensities $[(C_p - \gamma_e T)/T^3]_{max}$ are listed in Table III.

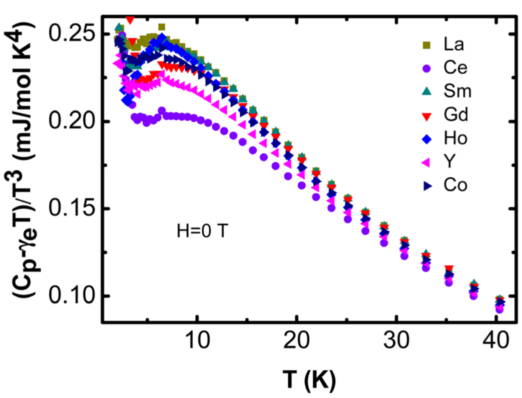

FIG. 6. (Color online) Boson heat capacity $(C_p - \gamma_e T)/T^3$ vs T of $(CuZr)_{92.5}Al_7X_{0.5}$ (X = La, Ce, Sm, Gd, Ho, Y, and Co) BMGs after subtracting the electronic contribution and/or the magnetic contribution.

As shown in Fig. 6, the maximum boson heat capacity and peak temperatures of $(CuZr)_{92.5}Al_7X_{0.5}$ (X = La, Ho, Sm, Co, Gd, and Y) BMGs change with the different elements addition. It is widely recognized that boson peaks correlate with low frequency vibration modes of loose atoms, clusters, or weakly bonded ions.[36,37] High intensity of boson peak corresponding to high density of low frequency vibration states indicates large free volume in the BMGs.[38] The relatively small intensity of boson specific heat for $(CuZr)_{92.5}Al_7Ce_{0.5}$ BMG according to our data shown in Fig. 6 might be caused by the strong hybridization between 4*f* electrons and itinerant electrons at low temperatures.[35]

Considering shear modulus $G = \rho v_t^2$, boson peak frequency associated with the van Hove singularities can be expressed as $\omega_{BZ} = 2v_t/a$, where v_t is the speed of transverse wave and a is the distance between two adjacent unit cells.[39,40] So boson specific heat peak temperatures T_{max} are correlated with the speed of transverse wave v_t and atomic radiuses. Table III shows that the peak temperatures have a raising trend with decreasing atomic radii of doped elements for $(CuZr)_{92.5}Al_7X_{0.5}$ (X = La, Sm, and Y) BMGs. Relatively low T_{max} of $(CuZr)_{92.5}Al_7X_{0.5}$(X = Ho, Co, and Gd) BMGs could be correlated with large magnetic clusters or domains due to the large magnetic moments of Ho, Co, and Gd additional elements.

Table II lists the plasticity of $(CuZr)_{92.5}Al_7X_{0.5}$ (X = La, Sm, Ho, Co, Gd, and Y) BMGs. We define ε_s as the strain from the onset of serration to ultimate breaking as it is widely recognized that the serration corresponds to the generation and sliding of shear bands.[41] Figure 7(a) shows the relation between the ε_s and boson heat capacity peak intensities $[(C_p\text{-}\gamma_e T)/T^3]_{max}$ for $(CuZr)_{92.5}Al_7X_{0.5}$ (X = La, Sm, Ho, Co, Gd, and Y) BMGs. The ε_s increases with the declining of peak intensities $[(C_p\text{-}\gamma_e T)/T^3]_{max}$. This seems to indicate that the BMG with low boson peak intensities has high plasticity or large Poisson's ratio ν.[23,26] The speeds of transverse wave v_t, G and ν for $(CuZr)_{92.5}Al_7X_{0.5}$(X = La, Co, Y) BMGs are shown in Table IV (The data were obtained with the same method in Ref. 23.) We plotted ν versus boson heat capacity peak intensities for $(CuZr)_{92.5}Al_7X_{0.5}$ (X = La, Co,

TABLE III. Low temperature specific heat data of $(CuZr)_{92.5}Al_7X_{0.5}$ (X = La, Sm, Ce, Gd, Ho, Y, Co) BMGs. For $(CuZr)_{92.5}Al_7X_{0.5}$ (X = La, Y, Co) BMGs, we got Sommerfeld coefficient γ_e from the least-square linear fit of specific heat data with formula $C_p = \gamma_e T + \beta T^3$ below 10 K. For $(CuZr)_{92.5}Al_7X_{0.5}$ (X = Sm, Ce, Gd, Ho) BMGs, we obtained γ_e with formula $C_p = \gamma_e T + \beta T^3 + C$ in the low temperature range where Kondo/Schottky effect is small, in which C represents the constant contribution of magnetic clusters.

Alloys	γ_e (mJ/mol K^2)	β (mJ/mol K^4)	T_{max} (K)	$[(C_p\text{-}\gamma_e T)/T]_{max}$ (mJ/mol K^4)
$(CuZr)_{92.5}Al_7La_{0.5}$	3.21	0.241	6.46	0.254
$(CuZr)_{92.5}Al_7Sm_{0.5}$	3.36	0.240	6.48	0.246
$(CuZr)_{92.5}Al_7Ce_{0.5}$	3.52	0.203	6.46	0.206
$(CuZr)_{92.5}Al_7Gd_{0.5}$	4.36	0.229	6.47	0.233
$(CuZr)_{92.5}Al_7Ho_{0.5}$	4.85	0.225	6.47	0.248
$(CuZr)_{92.5}Al_7Y_{0.5}$	3.10	0.219	6.96	0.224
$(CuZr)_{92.5}Al_7Co_{0.5}$	3.12	0.232	6.48	0.242

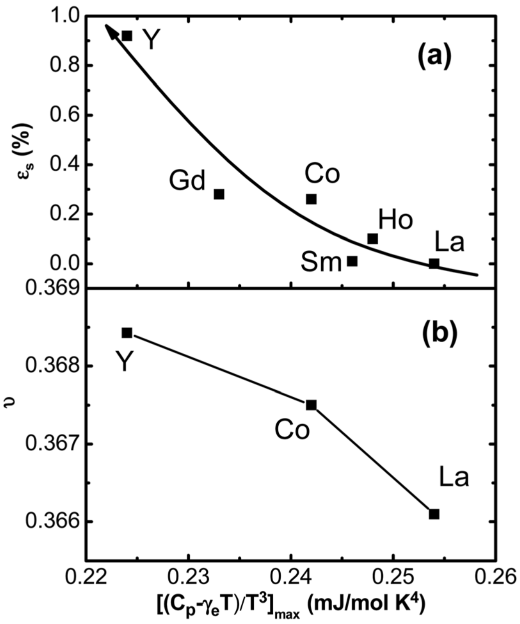

FIG. 7. (a) The strain from the onset of serration to ultimate fracture ε_s vs boson heat capacity peak intensity $[(C_p-\gamma_e T)/T^3]_{max}$ for $(CuZr)_{92.5}Al_7X_{0.5}$ (X = La, Sm, Ho, Co, Gd, and Y) BMGs. The curve with an arrow is drawn as a guide for the eyes. (b) Poisson's ratio ν vs boson heat capacity peak intensity $[(C_p-\gamma_e T)/T^3]_{max}$ for $(CuZr)_{92.5}Al_7X_{0.5}$ (X = La, Co, and Y) BMGs.

and Y) BMGs [see Fig. 7(b)]. It is indeed that the low boson peak intensities correspond to the BMGs with large ν. The $(CuZr)_{92.5}Al_7Ce_{0.5}$ BMG appears very brittle though the boson heat capacity peak is low.

2. Kondo screening effect

To explore the origin of the specific heat anomalies at low temperatures shown in Fig. 5, we studied the specific heat of all the BMGs under applied field of 1 T and 5 T. The low temperature C_p of $(CuZr)_{92.5}Al_7X_{0.5}$ (X = La, Y, and Co) BMGs (the additional elements have no 4*f* electrons) is independent of applied field while for $(CuZr)_{92.5}Al_7X_{0.5}$ (X = Ce, Sm, Gd, and Ho) BMGs (the additional elements have 4*f* electrons) the specific heat has evident variations with the changing field. Figure 8(a) shows the magnetic specific heat C_{mag} versus *T* for $(CuZr)_{92.5}Al_7Ce_{0.5}$ BMG, which was obtained by subtracting the specific heat of $(CuZr)_{92.5}Al_7La_{0.5}$ BMG from that of the studied BMG. The result is then scaled with the atomic percentage content of the added element. The C_{mag} of $(CuZr)_{92.5}Al_7Ce_{0.5}$ BMG at zero field should be caused by Kondo screening effect mainly as the interaction between Kondo and RKKY effect appears at lower temperatures due to very dilute Ce atoms.[42] Hybridization of 4*f* electrons near Fermi level and itinerant electrons reduces rotational degrees of freedom of Ce ions and the specific heat hump reflects the decreasing of magnetic states of Ce ions.[43] When the applied field increases, the peak of C_{mag} moves to a high temperature and becomes more pronounced, which can be attributed to the Zeeman splitting of the ground state.[44] At low fields a separated specific hump due to Schottky effect appears at a low temperature. The hump moves to high temperatures with increasing fields and merges with the Kondo heat capacity peak when the field energy approaches Kondo energy $k_B T_K$, where T_K is the Kondo temperature. At very high fields the free-spin Schottky resonance is asymptotically reached on a logarithmic scale and the merged hump tend to approach the free-spin Schottky anomaly.[45,46]

TABLE IV. Speeds of transverse wave v_t, shear modulus *G* and Poisson ratios ν for $(CuZr)_{92.5}Al_7X_{0.5}$ (X = La, Co, Y) BMGs.

Alloys	v_t (km/s)	*G* (GPa)	ν
$(CuZr)_{92.5}Al_7La_{0.5}$	2.12	31.8	0.3661
$(CuZr)_{92.5}Al_7Co_{0.5}$	2.18	33.7	0.3675
$(CuZr)_{92.5}Al_7Y_{0.5}$	2.16	33.2	0.3684

Figure 8(b) shows the temperature-dependent resistance of the $(CuZr)_{92.5}Al_7Ce_{0.5}$ BMG at zero field and 5 T. The resistance of the BMG rises slowly at about 20 K with decreasing temperature. Below 10 K, it rises quickly again due to spin-flip scattering of conductive electrons by the magnetic atoms. This behavior corresponds to the Kondo screening effect.[43]

Figure 8(c) presents the susceptibilities χ of Ce^{3+} ions in $(CuZr)_{92.5}Al_7Ce_{0.5}$ BMG, which shows Curie–Weiss regions at high temperatures. We fit the data in Curie–Weiss regions with the formula $N_A\mu_0\mu_{eff}^{exp}/[3k_B(T-\theta_p)]$, where N_A is the Avogadro's constant, μ_0 is the permeability of vacuum, μ_{eff}^{exp} is the effective moment of magnetic ion, k_B is the Boltzmann constant, θ_p is the paramagnetic Curie–Weiss temperature. The calculated effective magnetic moment of Ce^{3+} ions at 5 T is 1.13 μ_B, which is smaller than that at 0.5 T, 1.49 μ_B, and the theoretical value 2.54 μ_B. When applied field is 0.5 T, effective magnetic moments of Ce^{3+} ions begin to decrease below 70 K supposing magnetic susceptibilities still equal to $N_A\mu_0\mu_{eff}^{exp}/[3k_B(T-\theta_p)]$. This phenomenon originates from the formation of itinerant electronic clouds around Ce^{3+} ions, which is consistent with the specific heat anomalies of $(CuZr)_{92.5}Al_7Ce_{0.5}$ BMG at low applied field. As shown in Fig. 8(d) the maximum effective moment μ_{max} of Ce^{3+} ions at 1.6 K and 7 T is 0.40 μ_B/f.u, which is much smaller than the theoretical saturated value μ_{sat}^{theo} (2.14 μ_B/f.u) calculated using $\mu_{sat}^{theo} = [J/(J+1)]^{1/2}\mu_{eff}^{theo}$, where *J* is the total angular momentum at the ground state.[47] The phenomenon confirms that the Kondo screening effect exists in $(CuZr)_{92.5}Al_7Ce_{0.5}$ BMG. The field-dependent magnetization data at 1.6 K is different from those at 10 K which might indicate Schottky effect between 1.6 K and 10 K. We will discuss this in the next part. The maximum effective moment of Sm^{3+} ions at 1.6 K and 5 T is 0.21 μ_B/f.u, which is also much smaller than the theoretical saturated value of 0.71 μ_B/f.u. for $(CuZr)_{92.5}Al_7Sm_{0.5}$ BMG. The Kondo screening effect might also exist in $(CuZr)_{92.5}Al_7Sm_{0.5}$ BMG.

3. The Schottky anomalies

The magnetic specific heat C_{mag} versus *T* for $(CuZr)_{92.5}Al_7Gd_{0.5}$ BMG is shown in Fig. 9(a). A broad hump can be seen at low temperature and moves to about 8 K with the filed increasing from zero field to 5 T. The peak is most probably due to multi-level Schottky effect.[48,49] The Schottky

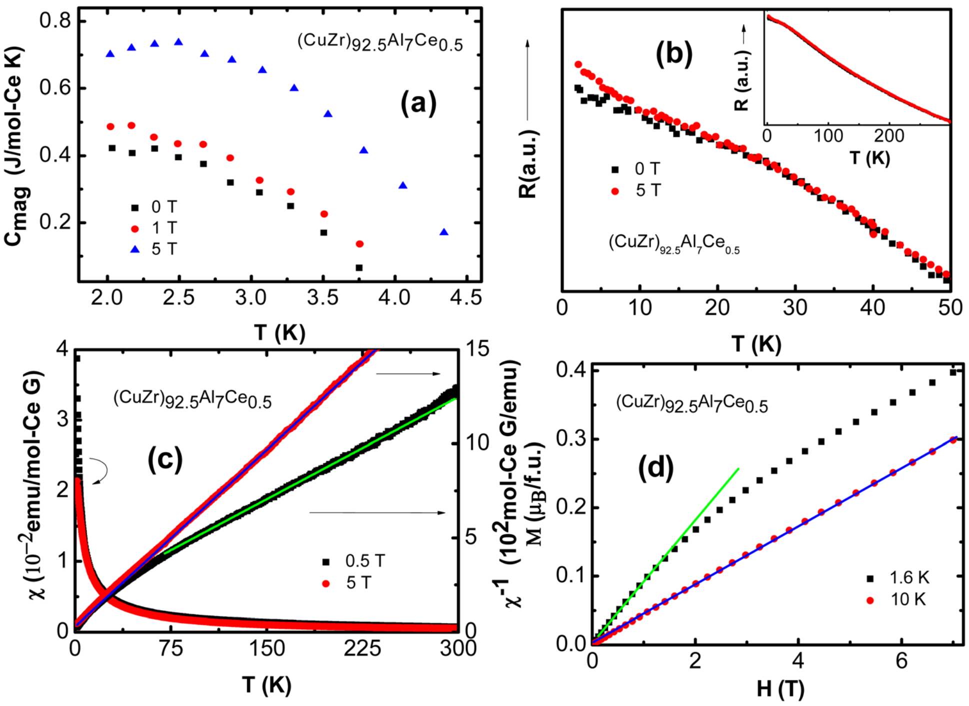

FIG. 8. (Color online) (a) Magnetic specific heat C_{mag} vs temperature T under applied field of 0, 1, 5 T for $(CuZr)_{92.5}Al_7Ce_{0.5}$ BMG. (b) The T-dependent resistance of $(CuZr)_{92.5}Al_7Ce_{0.5}$ BMG under applied field of 0 T and 5 T. (c) Susceptibility χ and inverse χ^{-1} vs T for $(CuZr)_{92.5}Al_7Ce_{0.5}$ BMG under applied field of 0.5 T and 5 T. (d) Magnetization M vs applied field H for $(CuZr)_{92.5}Al_7Ce_{0.5}$ BMG at 1.6 K and 10 K. The solid lines are fitting line.

effect often exists in paramagnetic salts and connects with specific heat C_S with particular characteristics.[34] When temperature is extremely large, C_S is proportional to T^{-2} while when temperature approaches absolute zero C_S increases exponentially.[43] The low temperature parts of the magnetic specific heat peak of $(CuZr)_{92.5}Al_7Gd_{0.5}$ BMG can be well fitted by $Ae^{-B/T}+C$ and high temperature tails can be fitted by $AT^{-2}+C$, where C represents specific heat contributed by magnetic clusters. Figure 9(b) shows the temperature-dependent resistance of the $(CuZr)_{92.5}Al_7Gd_{0.5}$ BMG at zero field and 5 T. The BMG displays positive magnetoresistive effect and no anomaly appears at low temperatures.

As shown in Fig. 9(c) Curie–Weiss susceptibilities χ of Gd^{3+} ions obey Curie–Weiss laws at high temperatures and the calculated effective moments μ_{eff}^{exp} are 7.88 μ_B at 0.1 T and 7.98 μ_B at 5 T, which are close to the theoretical value of 7.94 μ_B. At low temperatures when applied field increases to 5 T, the magnetic susceptibilities decrease and inverse susceptibilities show an upturn. The upturn exists in the same temperature range with that of the magnetic specific heat hump. This indicates that the upturn is associated with the Schottky effect. In Fig. 9(d), we show magnetization M versus applied field H for the BMG at low temperatures around the magnetic specific heat hump at 5 T. The maximum effective moments

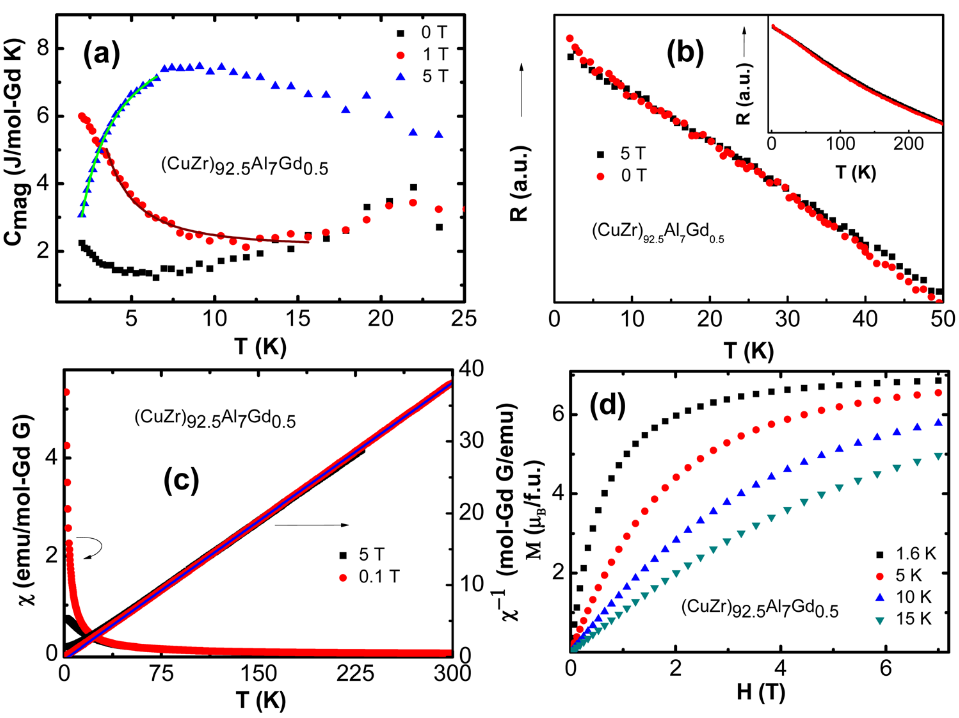

FIG. 9. (Color online) (a) Magnetic specific heat C_{mag} vs T under applied field of 0, 1, 5 T for $(CuZr)_{92.5}Al_7Gd_{0.5}$ BMG. The solid lines are the fitting results with $AT^{-2}+C$ and $Ae^{-B/T}+C$, respectively, where C represents specific heat contributed by magnetic clusters. (b) The T-dependent resistance of the BMG under applied field of 0 T and 5 T. (c) Susceptibility χ and χ^{-1} vs T for the BMG under 0.1 T and 5 T. (d) Magnetization M vs H for the BMGs at 1.6 K, 5 K, 10 K, and 15 K. The solid lines are the fitting line.

of Gd^{3+} ions at 1.6 K and 7 T are 6.86 μ_B/f.u, which is close to the theoretical saturated value 7.00 μ_B/f.u. This confirms that the low-temperature anomalies of $(CuZr)_{92.5}Al_7Gd_{0.5}$ BMG are not due to Kondo screening effect.

The origin of the Schottky effect in the Gd additional BMG can be explained by the change of magnetic states at different temperatures and fields. Far above the temperatures of the specific heat peaks, magnetic moments follow Boltzmann distribution at the $2J+1$ states and show paramagnetism.[50] Around peak temperatures more magnetic moments stay at low energy states and have larger projections in the direction of applied field,[27] and the magnetization of the rare earth ions will increase. At low temperature far below the specific heat peak temperature, more magnetic moments will stay at low energy states if applied fields are increased. In this procedure magnetization increases and magnetic susceptibilities decrease until the magnetization is saturated. The magnetization changes in Figs. 8(d) and 9(d) are consistent with that of Figs. 8(c) and 9(c).

The low-temperature properties of $(CuZr)_{92.5}Al_7Ho_{0.5}$ BMG are very similar to those of $(CuZr)_{92.5}Al_7Gd_{0.5}$ BMG. For $(CuZr)_{92.5}Al_7Sm_{0.5}$ BMG, the high temperature tail of the magnetic heat capacity hump at 5 T can be well fitted by $AT^{-2}+C$. At low temperatures when applied field increases to 5 T, its magnetic susceptibilities also decrease. The low-temperature anomalies of $(CuZr)_{92.5}Al_7Sm_{0.5}$ BMG may be related to Schottky effect as well.

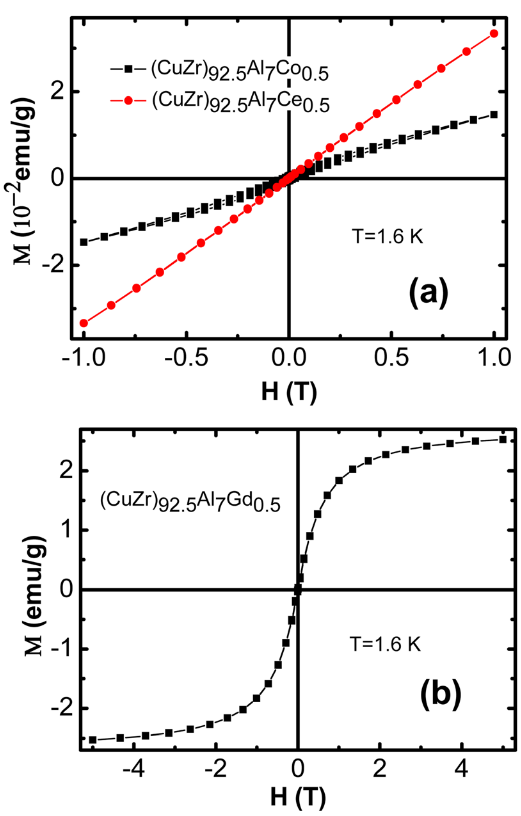

FIG. 10. (Color online) Magnetic hysteresis loops for (a) $(CuZr)_{92.5}Al_7Co_{0.5}$ and $(CuZr)_{92.5}Al_7Ce_{0.5}$, (d) $(CuZr)_{92.5}Al_7Gd_{0.5}$ BMG at 1.6 K.

4. Superparamagnetism and ferromagnetism

The minor addition with different rare earth elements induces different magnetic behaviors at low temperatures. Figure 10 shows the magnetic hysteresis loops at 1.6 K for $(CuZr)_{92.5}Al_7X_{0.5}$ (X = Co, Ce, and Gd) BMGs. It can be seen that $(CuZr)_{92.5}Al_7Co_{0.5}$, $(CuZr)_{92.5}Al_7Gd_{0.5}$ BMGs behave ferromagnetic and superparamagnetic at 1.6 K, respectively. Extremely small coercive forces and residual magnetization of minor rare earth element Gd doped BMGs indicate that magnetic clusters in them are smaller than the relative single magnetic domains with the sizes of several to tens of nanometers.[51] Obvious hysteresis of the magnetization curve for $(CuZr)_{92.5}Al_7Co_{0.5}$ BMG reveals that cobalt magnetic multidomain structures exist in this BMG.[47] $(CuZr)_{92.5}Al_7Ce_{0.5}$ BMG does not show ferromagnetism or superparamagnetism in the studied conditions, and its susceptibility changes slightly with increasing fields.

IV. CONCLUSIONS

We studied the effects of minor addition on formation, mechanical properties, and low temperature physical properties of $(CuZr)_{92.5}Al_7X_{0.5}$ (X = La, Ce, Sm, Gd, Ho, Y, and Co) BMGs. We find that the addition of rare earth elements can significantly change and modulate the formation, mechanical, and low temperature physical properties of the BMGs. The Young's modulus and ultimate stresses of our BMGs have an increasing trend with the atomic radii of added rare earth elements. The $(CuZr)_{92.5}Al_7Ce_{0.5}$ BMG shows Kondo screening effect at low temperatures, while the Schottky effect exists in $(CuZr)_{92.5}Al_7X_{0.5}$ (X = Ce, Sm, Gd, and Ho) BMGs and induces magnetic field-sensitive specific heat anomalies. Our research provides some new perspectives on the formation, mechanical properties, low temperature properties of BMGs and could help us to design metallic glasses with desirable properties.

ACKNOWLEDGMENTS

The financial support was from the MOST 973 of China (2010CB731603) and NSF of China (Grant Nos. 50731008 and 50921091). We thank J. Q. Wang, D. Q. Zhao, D. W. Ding, P. Wen, M. X. Pan, L. S. Huo, and S. K. Su for experimental assistance and helpful discussions.

[1]A. Inoue and N. Nishiyama, MRS Bull. **32**, 651 (2007).
[2]W. L. Johnson, JOM **54**, 40 (2002).
[3]W. H. Wang, Adv. Mater. **21**, 4524. (2009); J Appl. Phys. **110**, 053521 (2011).
[4]W. H. Wang, Prog. Mater. Sci. **52**, 540 (2007); Q. Luo and W.H. Wang, J. Non-Cryst. Solids **355**, 759 (2009); W. H. Wang, M. X. Pan, D. Q. Zhao, Y. Hu, an H. Y. Bai, J. Phys.: Condens. Matter **16**, 3719 (2004).
[5]H. B. Lou, X. D. Wang, F. Xu, S. Q. Ding, Q. P. Cao, K. Hono, and J. Z. Jiang, Appl. Phys. Lett. **99**, 051910 (2011).
[6]B. Zhang, D. Q. Zhao, M. X. Pan, W. H. Wang, and A. L. Greer, Phys. Rev. Lett. **94**, 205502 (2005).
[7]M. B. Tang, D. Q. Zhao, M. X. Pan, and W. H. Wang, Chin. Phys. Lett. **21**, 901 (2004).
[8]W. H. Wang, J. J. Lewandowski, and A. L. Greer, J. Mater. Res. **20**, 2307 (2005).
[9]D. Xu, B. Lohwongwatana, G. Duan, W. L. Johnson, and C. Garland, Acta Mater. **52**, 2621 (2004).
[10]D. Wang, K. Lu, and Y. Li, Appl. Phys. Lett. **84**, 4029 (2004).

[11]N. Mattern, A. Schöps, U. Kühn, J. Acker, O. Khvostikova, and J. Eckert, J. Non-Cryst. Solids **354**, 1504 (2008).
[12]A. Pãduraru, U. G. Andersen, A. Thyssen, N. P. Bailey, K. W. Jacobsen, and J. Schiøtz, Mater. Sci. Eng. A **18**, 055006 (2010).
[13]J. Das, M. B. Tang, K. B. Kim, R. Theissmann, F. Baier, W. H. Wang, and J. Eckert, Phys. Rev. Lett. **94**, 205501 (2005).
[14]H. L. Peng, M. Z. Li, W. H. Wang, C. Z. Wang, and K. M. Ho, Appl. Phys. Lett. **96**, 021901 (2010).
[15]H. L. Peng, M. Z. Li, and W. H. Wang, Phys. Rev. Lett. **106**, 135503 (2011).
[16]Y. Zhang, D. Q. Zhao, R. J. Wang, M. X. Pan, and W. H. Wang, Mater. Trans. JIM **41**, 1410 (2000).
[17]Y. Xu, Y. L. Wang, X. J. Liu, G. L. Chen, and Y. Zhang, J. Mater. Sci. **44**, 3861 (2009).
[18]P. Yu, H. Y. Bai, and W. H. Wang, J. Mater. Res. **21**, 1674 (2006); J. Chen, Y. Zhang, J. P. He, K. F. Yao, B. C. Wei, and G. L. Chen, Scr. Mater. **54**, 1351 (2006).
[19]X. K. Xi, L. L. Li, B. Zhang, W. H. Wang, and Y. Wu, Phys. Rev. Lett. **99**, 095501 (2007).
[20]H. B. Yu, W. H. Wang, and H. Y. Bai, Appl. Phys. Lett. **92**, 081902 (2010).
[21]Y. H. Liu, G. Wang, R. J. Wang, D. Q. Zhao, M. X. Pan, and W. H. Wang, Science **315**, 1385 (2007).
[22]J. Pan, K. C. Chan, Q. Chen, N. Lia, S. F. Guo, and L. Liu, J. Alloys Compounds **504S**, S74 (2010).
[23]P. Yu and H. Y. Bai, Mater. Sci. Eng. A **485**, 1 (2008).
[24]M. B. Tang, H. Y. Bai, and W. H. Wang, Phys. Rev. B **72**, 012202 (2005).
[25]Y. Li, P. Yu, and H. Y. Bai, Appl. Phys. Lett. **86**, 231909 (2005).
[26]Y. Li, H. Y. Bai, and W. H. Wang, Phys. Rev. B **74**, 052201 (2006).
[27]R. S. Shankland, *Atomic and Nuclear Physics*, 2nd ed. (Macmillan, New York, 1960).
[28]K. Yosida, *Theory of Magnetism* (Springer, Berlin, 1996).
[29]A. Takeuchi and A. Inoue, Mater. Trans. **46**, 2817 (2005).
[30]D. R. Askel, P. P. Fulay, and W. J. Wright. *The Science and Engineering of Materials* (Cengage Learning, Stamford, 2010).
[31]G. M. Hua and D. Y. Li, Appl. Phys. Lett. **99**, 041907 (2011).
[32]P. Strange, A. Svane, W. M. Temmerman, Z. Szotek, and H. Winter, Nature **399**, 756 (1999).
[33]K. Schroder, J. Appl. Phys., **32**, 880 (1961).
[34]A. Tari, *The Specific Heat of Matter at Low Temperatures* (Imperial College Press, London, 2003).
[35]A. C. Hewson, *The Kondo Problem to Heavy Fermions* (Cambridge University Press, Cambridge, 1997).
[36]C. A. Angell, Y. Z. Yue, L. M. Wang, J. R. D. Copley, S. Borick, and S. Mossa, J. Phys.: Condens. Matter. **15**, S1051 (2003).
[37]G. D'Angelo, G. Carini, C. Crupi, M. Koza, G. Tripodo, and C. Vasi, Phys. Rev. B **79**, 014206 (2009).
[38]H. Shintani and H. Tanaka, Nature Mater. **7**, 870 (2008).
[39]D. J. Safarik, R. B. Schwarz, and M. F. Hundley, Phys. Rev. Lett. **96**, 195902 (2006).
[40]A. I. Chumakov, G. Monaco, A. Monaco, W. A. Crichton, A. Bosak, R. Rüffer, A. Meyer, F. Kargl, L. Comez, D. Fioretto, H. Giefers, S. Roitsch, G. Wortmann, M. H. Manghnani, A. Hushur, Q. Williams, J. Balogh, K. Parliński, P. Jochym, and P. Piekarz, Phys. Rev. Lett. **106**, 225501 (2011).
[41]H. M. Chen, J. C. Huang, S. X. Song, T. G. Nieh, and J. S. C. Jang, Appl. Phys. Lett. **94**, 141914 (2009).
[42]M. B. Tang, H. Y. Bai, and W. H. Wang, Phys. Rev. B **75**, 172201 (2007).
[43]C. Enss and S. Hunklinger, *Low-Temperature Physics* (Springer, Berlin, 2005).
[44]H. P. van der Meulen, A. de Visser, J. J. M. Franse, T. T. J. M. Berendschot, J. A. A. J. Perenboom, H. van Kempen, A. Lacerda, P. Lejay, and J. Flouquet, Phys. Rev. B **44**, 814 (1991).
[45]V. T. Rajan, J. H. Lowenstein, and N. Andrei, Phys. Rev. Lett. **49**, 497 (1982).
[46]P. D. Sacramento and P. Schlottmann, Phys. Rev. B. **43**, 13294 (1991).
[47]C. Kittel, *Introduction to Solid State Physics*, 7th ed. (John Wiley & Sons, New York, 1996).
[48]W. E. Wallace, S. G. Sankar, and V. U. S. Rao, Struct. Bonding **33**, 1 (1977).
[49]D. J. Germano and R. A. Butera, Phys. Rev. B **24**, 3912 (1981).
[50]P. V. Panat, *Thermodynamics and Statistical Mechanics* (Alpha Science, Oxford, 2008).
[51]U. Jeong, X. Teng, Y. Wang, H. Yang, and Y. Xia, Adv. Mater. **19**, 33 (2007).